Supporting Information

Synthesis, structure and bonding of actinide disulphide dications, AnS_2^{2+}, in the gas phase

Ana F. Lucena,[1] Nuno A. G. Bandeira,[2,3,4,*] Cláudia C. L. Pereira,[1,§]
John K. Gibson,[5] Joaquim Marçalo[1,*]

[1] *Centro de Ciências e Tecnologias Nucleares, Instituto Superior Técnico, Universidade de Lisboa, Estrada Nacional 10 (km 139,7), 2695-066 Bobadela LRS, Portugal*

[2] *Institute of Chemical Research of Catalonia (ICIQ), Barcelona Institute of Technology (BIST), 16 – Av. Països Catalans, 43007 Tarragona, Spain*

[3] *Centro de Química Estrutural, Instituto Superior Técnico, Universidade de Lisboa, Av. Rovisco Pais 1, 1049-001 Lisboa, Portugal*

[4] *Centro de Química e Bioquímica, Faculdade de Ciências, Universidade de Lisboa, Campo Grande, 1749-016 Lisboa, Portugal*

[5] *Chemical Sciences Division, Lawrence Berkeley National Laboratory, Berkeley, California 94720, United States*

[§] Present address: *REQUIMTE, Faculdade de Ciências e Tecnologia, Universidade Nova de Lisboa, 2829-516 Caparica, Portugal*

* Corresponding authors: Nuno A. G. Bandeira, email: nbandeira@iciq.es; Joaquim Marçalo, email: jmarcalo@ctn.tecnico.ulisboa.pt

Contents:

Experimental details.

Table S1 - Reaction products and kinetics for the reactions of AnS_2^{2+} and AnS_3^{2+} with COS.

Figure S1 - Calculated geometries of the ground states of di-haptic actinide sulphides: η^2-ThS_2^{2+} (MP2), η^2-US_2^{2+} [CASPT2(4,8)], η^2-NpS_2^{2+} [CASPT2(5,8)] and η^2-PuS_2^{2+} [CASPT2(6,8)].

Table S2 - Main data from the CASPT2(4,8) optimisation of η^2-UO_2^{2+}.

Table S3 - Main data from the CASPT2(13,13) single point calculation of η^2-NpS_2^{2+}.

Table S4 - MO composition of the main bonding orbitals in η^2-AnS_2^{2+} extracted from the corresponding CASPT2(n,13) wavefunction.

Figure S2 - Active space MOs used in the energy calculation of triangular species, such as η^2-NpS_2^{2+} seen here, used in the CASPT2(13,13) calculations.

Table S5 - Mayer Bond Order (MBO) values of each ground state geometry calculated with the CASPT2(n,13) method.

Table S6 - MO symmetry species and corresponding axis frame definition used in the symmetry constrained calculations.

Table S7 - CASPT2(n,13) energies (a.u.) of the symmetrised (C_{2v}) minima in each spin class with respective term symbols.

Figure S3 - State relative energies for each isomer class in $[SAnS]^{2+}$ and η^2-$[AnS_2]^{2+}$ cations (An = Np, Pu).

Experimental details

Gas-phase experiments were performed by Fourier transform ion cyclotron resonance mass spectrometry (FTICR-MS) in a Extrel/Finnigan FT/MS 2001 - DT spectrometer, equipped with a 3 Tesla superconducting magnet, a Spectra-Physics Quanta-Ray GCR-11 Nd:YAG laser operated at the fundamental wavelength (1064 nm), and a Finnigan Venus Odyssey data system. The An^{2+} ions were produced by direct laser desorption/ionization (LDI) of small pieces of alloys that contained ~20% of Th or ~5% of the remaining actinide metals (Np, Pu, Am, Cm) in a Pt matrix, mounted on the solids probe of the instrument. All ion manipulations were conducted in the source cell of the dual cell instrument. Ion selection was achieved using single-frequency, frequency-sweep, or SWIFT excitation.[a] The COS reagent was a commercial product with >99% purity as confirmed by electron ionization mass spectra. COS was introduced into the spectrometer through a leak valve to pressures of (1-3)x10^{-7} Torr, measured with a Bayard-Alpert type ionization gauge. The gauge readings were corrected for the relative sensitivity of the reagent, calculated according to the procedure of Bartmess and Georgiadis,[b] based on the experimental molecular polarizability.[c] The pressures in the cell were calibrated using standard reactions of methane and acetone ions.[d,e] The background in the spectrometer mainly consisted of water and air, with base pressures lower than (1-2)x10^{-8} Torr, that is, at least one order of magnitude lower than the reagent pressures used. The reactant ions were thermalized by collisions with argon, which was introduced into the spectrometer through a leak valve to constant pressures in the range of (1-5)x10^{-6} Torr. Indications that effective thermalization had been achieved came from the reproducibility of the reaction kinetics and product distributions for different collisional cooling periods or collision gas pressures, and from the linearity of the pseudo-first-order kinetics plots. The reactant An^{2+} ions or sequential product ions were isolated in the cell, and product ion intensities were monitored as a function of the reaction time. Rate constants, k, were determined from the pseudo-first-order decay of the relative signals of the reactant ions as a function of time at constant neutral pressures. Along with the absolute rate constants, k, and for comparative purposes, reaction efficiencies are described as k/k_{COL}, where the k_{COL} is the collisional rate constant derived from the modified variational transition state/classical trajectory theory developed by Su and Chesnavich.[f] Collisional rate constants were calculated using the experimental molecular polarizability and dipole moment of COS.[c] The main source of uncertainty in the absolute rate constants is the pressure measurement, and errors up to ±50% are usually assigned to them. Relative rate constants for different reactions are estimated to be accurate to ±20%, while typical precisions for replicate measurements of the same reaction are ±10%. The detection limit for most reactions was $k/k_{COL} \leq 0.005$.

[a] Guan, S. H.; Marshall, A. G., Stored waveform inverse Fourier transform (SWIFT) ion excitation in trapped-ion mass spectometry: Theory and applications, *International Journal of Mass Spectrometry and Ion Processes* **1996**, *157*, 5.

[b] Bartmess, J. E.; Georgiadis, R. M., Empirical-methods for determination of ionization gauge relative sensitivities for different gases, *Vacuum* **1983**, *33*, 149.

[c] Lide, D. R. (Ed.), *CRC Handbook of Chemistry and Physics*, 90th ed.; CRC Press: Boca Raton, FL, 2009.

[d] Bruce, J. E.; Eyler, J. R., Probing trapped ion energies via ion-molecule reaction-kinetics - Fourier transform ion-cyclotron resonance mass spectrometry, *Journal of the American Society for Mass Spectrometry* **1992**, *3*, 727.

[e] Yi, L.; Ridge, D. P.; Munson, B., Association reactions of trimethylsilyl ions, *Organic Mass Spectrometry* **1991**, *26*, 550.

[f] Su, T.; Chesnavich, W. J., Parametrization of the ion-polar molecule collision rate-constant by trajectory calculations, *Journal of Chemical Physics* **1982**, *76*, 5183.

Table S1. Reaction products and kinetics for the reactions of AnS_2^{2+} and AnS_3^{2+} with COS[a]

Reactant ion	**Products**	k/k_{COL} **[**k**]**	**Reactant ion**	**Products**	k/k_{COL} **[**k**]**
$\mathbf{ThS_2^{2+}}$	ThS_3^{2+} (100%)	0.42 [0.81]	$\mathbf{ThS_3^{2+}}$	ThS_4^{2+} (100%)	0.25 [0.48]
$\mathbf{US_2^{2+}}$	US_3^{2+} (45%)	0.36 [0.69]	$\mathbf{US_3^{2+}}$	US_4^{2+} (75%)	0.36 [0.67]
	US_2^+ (15%)			UOS_2^+ (25%)	
	UOS^+ (40%)				
$\mathbf{NpS_2^{2+}}$	NpS_3^{2+} (45%)	0.18 [0.34]	$\mathbf{NpS_3^{2+}}$	?	?
	NpS_2^+ (55%)				

[a] Where more than one product was observed, the relative yields are given in parentheses; the pseudo-first-order rates are expressed as reaction efficiencies, k/k_{COL}, and in brackets as absolute rates, $k/10^{-9}$ cm^3 $molecule^{-1}$ s^{-1}; the data for uranium are from: Pereira et al. *Inorg. Chem.* **2013**, *52*, 14162-14167; the reactivity of NpS_3^{2+} could not be studied due to poor ion signal.

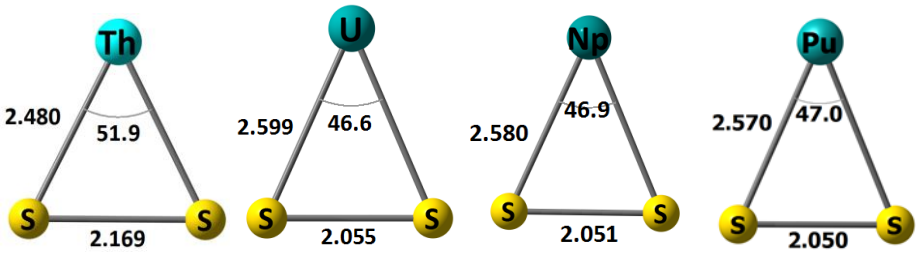

Figure S1. Calculated geometries of the ground states of di-haptic actinide sulphides: η^2-ThS_2^{2+} (MP2), η^2-US_2^{2+} [CASPT2(4,8)], η^2-NpS_2^{2+} [CASPT2(5,8)] and η^2-PuS_2^{2+} [CASPT2(6,8)] (bond distances in angstroms and bond angles in degrees).

Table S2 - Main data from the CASPT2(4,8) optimisation of η^2-UO_2^{2+}.

Total Spin	**1**	**2**
ΔE (kcal mol^{-1})	0	+5.1
d(U-O)/Å	2.146	2.195
d(O-O)/Å	1.306	1.314
(5f$_{\delta 1}$+)π^-	1.132	1.000*
5f$_\sigma$	0.932	0.015
5f$_{\varphi 1}$	0.796	0.261
5f$_{\pi 1}$	0.060	0.912
5f$_{\varphi 2}$	0.184	0.736
5f$_{\delta 2}$	0.203	0.787
5f$_{\delta 1}$($-\pi^-$)	0.674	0.214*
5f$_{\pi 2}$	0.0	0.075

* Fully localised orbitals, orbital in brackets does not contribute.

Table S3. Main data from the CASPT2(13,13) single point calculation of η^2-NpS_2^{2+}.

Total Spin	**3/2**	**5/2**
$\Delta E(kcal\ mol^{-1})$	0	+3.4
σ^+	1.969	1.969
π_1^+	1.999	1.999
π_2^+	1.980	1.980
$(5f_{\delta 1}+)\pi_1^-$	1.155	1.019*
π_2^-	1.993	1.995
σ^-	0.037	0.036
$5f_{\delta 1}(-\pi^-)$	0.769	0.930*
$5f_{\delta 2}$	0.862	0.065
$5f_{\varphi 1}$	0.970	0.963
$5f_{\varphi 2}$	0.077	0.957
$5f_{\pi 1}$	0.126	0.078
$5f_{\pi 2}$	0.135	0.101
$5f_{\sigma}$	0.930	0.908

* Fully localised orbitals, orbital in brackets does not contribute.

Table S4. MO composition of the main bonding orbitals in η^2-AnS_2^{2+} extracted from the corresponding CASPT2(n,13) wavefunction.

		$6d_\sigma+\sigma^-$ 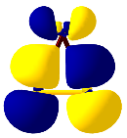	$5f_{\delta 1}+\pi^-$ 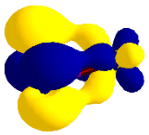	$5f_{\delta 1}-\pi^-$ 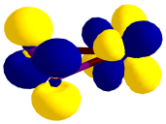
			η^2-ThS_2^{2+}	
%S		72.5	81.5	37.5
%Th		27.5	18.5	62.5
	%5f	3.2	3.5	9.2
	%6d	22.8	14.8	50.3
			η^2-US_2^{2+}	
%S		83.3	89.1	13.5
%U		16.7	10.9	86.5
	%5f	1.9	9.9	85.6
	%6d	12.3	0.8	0.7
			η^2-NpS_2^{2+}	
%S		80.2	66.6	38.1
%Np		19.8	33.4	61.9
	%5f	2.2	32.6	60.7
	%6d	13.8	0.7	1.0
			η^2-PuS_2^{2+}	
%S		84.3	70.4	34.6
%Pu		15.7	29.6	65.4
	%5f	2.1	28.8	64.4
	%6d	11.5	0.7	0.7

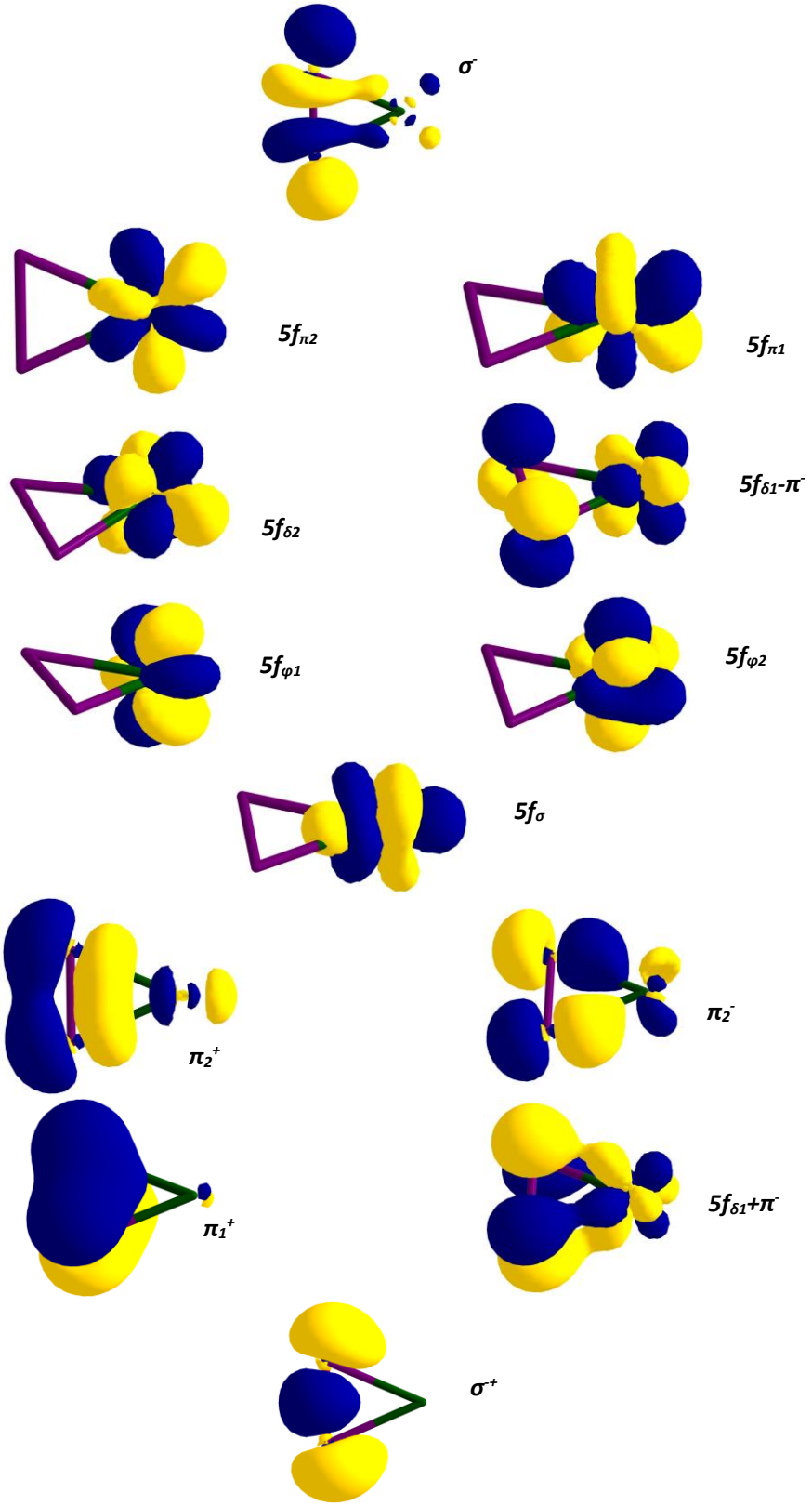

Figure S2. Nature of the extended active space MOs used in the energy calculation of triangular species, such as η^2-NpS_2^{2+} seen here, used in the CASPT2(13,13) calculations.

Table S5. Mayer Bond Order (MBO) values of each ground state geometry calculated with the CASPT2(n,13) method.

An	MBO An-S ($[SAnS]^{2+}$)	MBO An-S (η^2-$[AnS_2]^{2+}$)	MBO S-S (η^2-$[AnS_2]^{2+}$)
Th	2.19	1.66	0.80
U	2.49	1.03	1.07
Np	2.08	0.98	1.07
Pu	1.79	0.97	1.06

Table S6. MO symmetry species and corresponding axis frame definition used in the symmetry constrained calculations.

C_{2v} irrep subspecies	η^2-$[AnS_2]^{2+}$	$[SAnS]^{2+}$
a_1	$5f_{\sigma}$	$5f_{\varphi 1}$
	$5f_{\delta 2}$	$5f_{\pi 1} + \pi_1^+$
	σ^+	$5f_{\pi 1} - \pi_1^+$
	π_2^+	σ^+
b_1	π_1^+	$5f_{\pi 2} + \pi_2^+$
	$5f_{\varphi 1}$	$5f_{\varphi 2}$
	$5f_{\pi 1}$	$5f_{\pi 2} - \pi_2^+$
a_2	$5f_{\delta 1}(-\pi_1^-)$	$5f_{\delta 1}$
	$(5f_{\delta 1}+)\pi_1^-$	π_1^-
b_2	π_2^-	$5f_{\sigma}$-σ^-
	σ^-	π_2^-
	$5f_{\pi 2}$	$5f_{\delta 2}$
	$5f_{\varphi 2}$	$5f_{\sigma} + \sigma^-$

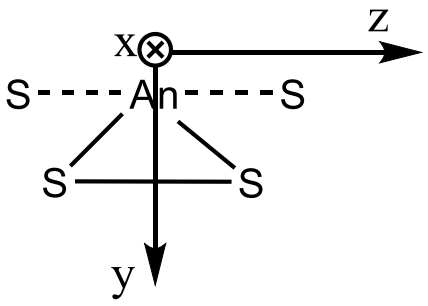

Table S7. CASPT2(n,13) energies (a.u.) of the symmetrised (C_{2v}) minima in each spin class with respective term symbols. Zeroth order reference weight in the perturbed wavefunction is added for each state.

States	$[SNpS]^{2+}$	ref. weight in PT2	η^2-$[NpS_2]^{2+}$	ref. weight in PT2
$^6A_1$			-29534.2050623	0.812
$^6B_1$			-29534.2065802	0.803
$^6A_2$			-29534.2074815	0.803
$^6B_2$			-29534.2072060	0.808
$^4A_1$	-29534.1995423	0.762	-29534.2097292	0.808
$^4B_1$	-29534.1995493	0.762	-29534.2115247	0.800
$^4A_2$	-29534.1892254	0.759	-29534.2113886	0.800
$^4B_2$	-29534.1597969	0.771	-29534.2112512	0.805
$^2A_1$	-29534.1924794	0.765	-29534.1595791	0.792
$^2B_1$	-29534.1924513	0.765	-29534.1567603	0.796
$^2A_2$	-29534.1799609	0.762	-29534.1594889	0.786
$^2B_2$	-29534.1788721	0.761	-29534.1600237	0.792
	$[SPuS]^{2+}$		η^2-$[PuS_2]^{2+}$	
$^7A_1$	-30336.5589586	0.752	-30336.6380591	0.809
$^7B_1$	-30336.5589071	0.752	-30336.6415324	0.805
$^7A_2$	-30336.5658118	0.752	-30336.6639494	0.793
$^7B_2$	-30336.5639264	0.758	-30336.6458541	0.796
$^5A_1$	-30336.6101511	0.752	-30336.6464738	0.803
$^5B_1$	-30336.6100967	0.752	-30336.6486027	0.799
$^5A_2$	-30336.6197838	0.752	-30336.6488876	0.797
$^5B_2$	-30336.6141209	0.762	-30336.6431409	0.793
$^3A_1$	-30336.5742103	0.753	-30336.5808391	0.797
$^3B_1$	-30336.6076222	0.753	-30336.5914473	0.789
$^3A_2$	-30336.6184739	0.754	-30336.5802545	0.793
$^3B_2$	-30336.6184829	0.754	-30336.5849501	0.799

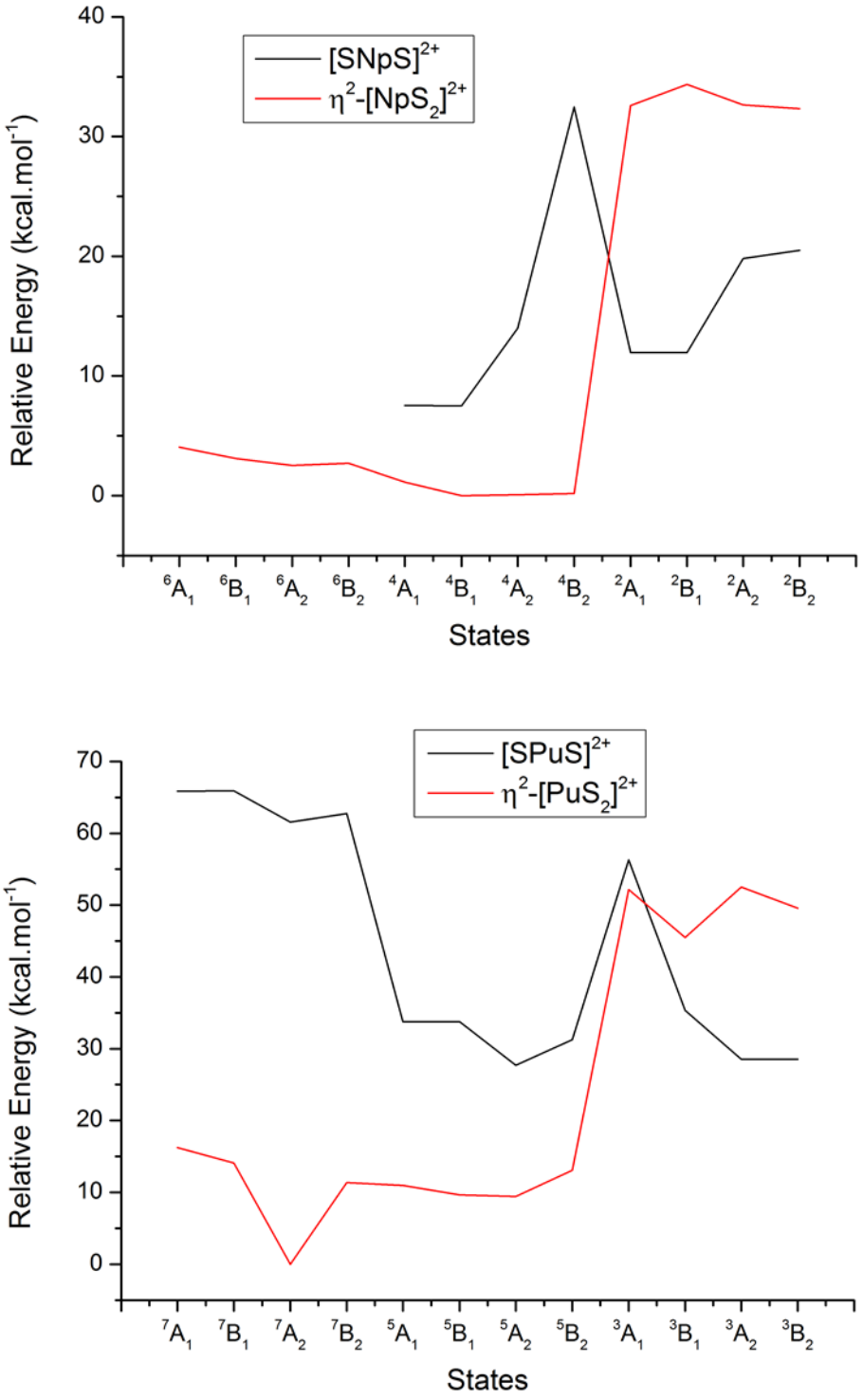

Figure S3. State relative energies for each isomer class in $[SAnS]^{2+}$ and η^2-$[AnS_2]^{2+}$ cations (An = Np, Pu).